nature astronomy

SUPPLEMENTARY INFORMATION

https://doi.org/10.1038/s41550-019-0914-9

In the format provided by the authors and unedited.

A complex storm system in Saturn's north polar atmosphere in 2018

A. Sánchez-Lavega[1]*, E. García-Melendo[2]*, J. Legarreta[3], R. Hueso[1], T. del Río-Gaztelurrutia[1], J. F. Sanz-Requena[4,5], S. Pérez-Hoyos[1], A. A. Simon[6], M. H. Wong[7], M. Soria[8], J. M. Gómez-Forrellad[9], T. Barry[10], M. Delcroix[11], K. M. Sayanagi[12], J. J. Blalock[12], J. L. Gunnarson[12], U. Dyudina[13] and S. Ewald[13]

[1]Departamento Física Aplicada I, Escuela de Ingeniería de Bilbao, Universidad del País Vasco UPV/EHU, Bilbao, Spain. [2]Serra Húnter Fellow, Escola Superior d'Enginyeries Industrial, Aeroespacial i Audiovisual, UPC, Terrasa, Spain. [3]Departamento de Ingeniería de Sistemas y Automática, Escuela de Ingeniería de Bilbao, Universidad del País Vasco UPV/EHU, Bilbao, Spain. [4]Departamento de Ciencias Experimentales, Universidad Europea Miguel de Cervantes, Valladolid, Spain. [5]Departamento de Física Teórica, Atómica y Optica; Facultad de Ciencas, Universidad de Valladolid, Valladolid, Spain. [6]NASA Goddard Space Flight Center, Greenbelt, MD, USA. [7]University of California Berkeley, Berkeley, CA, USA. [8]Escola Superior d'Enginyeries Industrial, Aeroespacial i Audiovisual, UPC, Terrasa, Spain. [9]Fundació Observatory Esteve Duran, Barcelona, Spain. [10]Broken Hill Observatory, Broken Hill, New South Wales, Australia. [11]Societé Astronomique de France, Paris, France. [12]Hampton University, Hampton, VA, USA. [13]California Institute of Technology, Pasadena, CA, USA. *e-mail: agustin.sanchez@ehu.eus; enrique.garcia.melendo@upc.edu

Supplementary Information File

A complex storm system in Saturn's north polar atmosphere in 2018

A. Sánchez-Lavega[1], E. García-Melendo[2], J. Legarreta[3], R. Hueso[1], T. del Río-Gaztelurrutia[1], J. F. Sanz-Requena[4-5], S. Pérez-Hoyos[1], A. A. Simon[6], M. H. Wong[7], M. Soria[8], J. M. Gómez-Forrellad[9], T. Barry[10], M. Delcroix[11], K. M. Sayanagi[12], J. J. Blalock[12], J. L. Gunnarson[12], U. Dyudina[13], S. Ewald[13]

1. Departamento Física Aplicada I, Escuela de Ingeniería de Bilbao, Universidad del País Vasco UPV/EHU, 48013 Bilbao, Spain (agustin.sanchez@ehu.eus)
2. Serra Húnter Fellow, Escola Superior d'Enginyeries Industrial, Aeroespacial i Audiovisual, UPC, Terrasa, Spain,
3. Departamento de Ingeniería de Sistemas y Automática, Escuela de Ingeniería de Bilbao, Universidad del País Vasco UPV/EHU, 48013 Bilbao, Spain
4. Departamento de Ciencias Experimentales. Universidad Europea Miguel de Cervantes, Valladolid, Spain
5. Departamento de Física Teórica, Atómica y Optica; Facultad de Ciencas, Universidad de Valladolid, Valladolid, Spain
6. NASA Goddard Space Flight Center, Greenbelt, MD, USA
7. University of California Berkeley, Berkeley, CA, USA,
8. Escola Superior d'Enginyeries Industrial, Aeroespacial i Audiovisual, UPC, Terrasa, Spain,
9. Fundació Observatory Esteve Duran, Barcelona, Spain
10. Astronomical Society of New South Wales, Sydney, New South Wales, Australia
11. Societé Astronomique de France, Paris, France.
12. Hampton University, VA, USA
13. California Institute of Technology, Pasadena, CA, USA

Contents:

Supplementary Table 1

List of observers whose images have been used in this study

In most cases, only the one or two best images per Saturnian rotation have been selected; number of days hence indicates for how many different Saturnian days an image from each observer was used. For instruments descriptions, SC stands for Schmidt Cassegrain, DK for Dall-Kirkham Cassegrain, RC for Ritchey Chretien, Do for Dobsonian, R refractor, (*) Chilescope

Images are available at:

- Planetary Virtual Observatory Laboratory: http://pvol2.ehu.eus/pvol2/
- Association of Lunar and Planetary Observers of Japan: http://alpo-j.asahikawa-med.ac.jp/Latest/index.html
- French Astronomical Society planets image gallery: http://astrosurf.com/planetessaf/saturne/index_en.htm
- Facebook Astronomy Planetary Imaging group: https://www.facebook.com/groups/204436579601722/

Observer	Country	Instrument	Filters	Days
Luis Amiama Gomez	Santo Domingo	SC 200 mm	R,G,B	2
Tomio Akutsu	Japan	SC 354mm	UBV,R,G,B,IR685,CH4	1
Christofer M. Baez	Santo Domingo	Newton 203mm	R,G,B	2
Trevor Barry	Australia	Newton 408mm	R,G,B,IR685,CH4	33
Bernard Bayle	France	SC 280mm	L	1
Jose A. Berdejo	Spain	SC 280mm	R,G,B	2
Guillaume Bertrand	France	Newton 254mm	L,IR740	1
Ioannis Bouhras	Greece	Newton 180mm	L	1
Stefan Buda	Australia	DK 405mm	R,G,B	1
Joaquin Camarena	Spain	SC 354mm	R,G,B,IR685	15
David Carlish	USA	Newton 406mm	L,IR742	6
Andy Casely	Australia	SC 354mm	R,G,B,R642,CH4	25
Alan Coffelt	USA	SC 280mm	L	1
Jean-Luc Dauvergne	France	DK 210mm	L,R,G,B	4
Marc Delcroix	France	Newton 320mm	R,G,B,R642	8
Kolovos Dimitrios	Greece	SC 280mm	R,G,B	2
Pericles Enache	Brazil	SC 280mm	R,G,B	12
Bernard Fouquet	France	Newton 305mm	L, IR760	2
Clyde Foster	South Africa	SC 354mm	R,G,B,IR	29
Bernd Gährken	Germany	Newton 711mm	R,G,B,IR	1
Christopher Go	Philippines	SC 354mm	R,G,B,IR	7
Guilherme Grassmann	Brazil	Newton 305 mm	R,G,B	2
Paul Haese	Australia	SC 354mm	R,G,B	1
Hidetugu Hashino	Japan	Newton 305 mm	R,G,B	3
Akitoshi Hatanaka	Japan	Newton 400mm	R,G.B	1
Robert Heffner	Japan	SC 235mm	R,G,B	1
Tadashi Horiuchi	Japan	Newton 406 mm	R,G,B	9
Rik Hill	USA	Mak 200mm	L	1

Mike Hood	USA	R 200mm	R,G,B	1
Toshihiko Ikemura	Japan	Newton 380 mm	R,G,B	1
Osamu Inoue	Japan	SC 280mm	L,R,G,B	1
Tutomu Ishibashi	Japan	Newton 310 mm	R,G,B	1
Ryuichi Iwamasa	Japan	SC 355 mm	L,R,G,B,CH4	3
Javier Beltran Jovani	Spain	Newton 508mm	L	2
Robert Jüptner-Jonstorff	Austria	SC 235mm	L	1
Dzmitry G. Kananovich	Chile (*)	RC 1000mm	R,G,B	2
Seiichi Kanno	Japan	Newton 300mm	R,G,B,IR685,CH4	1
Manos Kardasis	Greece	SC 354mm	R,G,B,R610,IR685,CH4	9
Szeto Koon Chuen	Hong Kong	Do 290 mm	R,G,B	1
Teruaki Kumamori	Japan	SC 355 mm	L,R,G,B	8
Carles Labordena	Spain	SC 235mm	R,G,B	1
Antonio Lasala	Spain	SC 280mm	R,G,B,IR	1
Michel Legrand	France	SC 280mm	R,G,B	1
Roch Levesque	Canada	DK 405mm	R,G,B	1
Martin Lewis	UK	Newton 440mm	L,R642,CH4	2
Mark Lonsdale	Australia	SC 280mm	R,G,B	1
Bruce MacDonald	USA	SC 354mm	L	41
John MacKeon	Ireland	SC 280mm	L,R,G,B	1
Kike Martin Ordiales	Spain	SC 280mm	R,G,B,IR742	
Walter Martins	Brazil	Newton 305 mm	R,G,B	4
Luis Martos	Spain	SC 280mm	L	1
Jim Melka	USA	Newton 450mm	R,G,B	1
Phil Miles	Australia	Newton 508mm	R,G,B,R610,IR700,CH4	3
Nobuya Minagawa	Japan	SC 235mm	R,G,B	3
Efrain Morales	Puerto-Rico	SC 305mm	R,G,B,IR685,CH4	12
Luigi Morrone	Italy	SC 280mm	R,G,B	3
Masaaki Nagase	Japan	SC 235mm	R,G,B	1
Tiziano Olivetti	Thaïland	DK 505mm	R,G,B,IR807	2
Tadao Ohsugi	Japan	Newton 300 mm	R,G,B	2
Damian Peach	Chile (*)	RC 1000mm	R,G,B	5
Sauveur Pedranghelu	France	SC 280mm	R,G,B	1
Christophe Pellier	France	Newton 305mm	R,G,B,R610,R642,IR685 IR740,IR800,CH4	11
William Pellissard	France	SC 354mm	IR	1
Darryl Pfintzer Milika	Australia	SC 354mm	R,G,B	4
Paul Rolet	France	Cassegrain 300mm	L	1
David Romero	Peru	SC 280mm	L	3
Amrit Seecharan	Trinidad	SC 235mm	L	1
Conrado Serodio	Brazil	Newton 305mm	R,G,B	3
Maciel Sparrenberger	Brazil	Newton 320mm	R,G,B	1
Avani Soares	Brazil	SC 354mm	L, IR685	5
Jose Soldevilla	Spain	SC 354mm	R,G,B	3
Emmanuel Sussenbach	Netherlands	SC 203mm	L,IR	7
Emilio Tortosa	Spain	Refractor 178mm	R,G,B	1
Troy Tranter	Australia			1
Sebastian Voltmer	Germany	Newton 711mm	R,G,B	1
Takahiro Yamaguchi	Japan	SC 235mm	R,G,B	1
Akihiro Yamazaki	Japan	SC 280mm	L,R,G,B	2
Tomoyuki Yoshida	Japan	DK 300mm	R,G,B	1
Kenkichi Yunoki	Japan	Newton 355 mm	R,G,B	1
Anthony Wesley	Australia	Newton 508mm	R,G,B,IR750	6
Leigh Westerland	Australia	SC 280mm	R,G,B	3
Michael Wong	Australia	Newton 305mm	R,G,B,IR685	5

Supplementary Table 2

Radiative Transfer model free and fixed parameters

Cloud/Haze	*Parameter*	*Type*	*A priori value*
Stratospheric Haze	P_1	Fixed	1 mbar
	P_2	Fixed	100 mbar
	τ	Free	0.01±0.01
	m_r	Fixed	1.43
	m_i	Fixed	0.001
	r_{eff}	Fixed	0.1 μm
	σ_{eff}	Fixed	0.1 μm
Tropospheric Haze	P_{top}	Free	600±100 mbar
	N	Free	20±10 cm^{-3}
	$H_{aerosol}/H_{gas}$	Free	10±0.1 km
	τ	Free	10±5
	r_{eff}	Free	1±0.5 μm
	σ_{eff}	Fixed	1.43
	m_r	Fixed	1.43
	m_i	Free	0.001±0.001
Cloud	P_5	Fixed	1 bar
	P_6	Fixed	1.4 bar
	τ	Free	10±5
	m_r	Fixed	1.43
	m_i	Fixed	0.001
	r_{eff}	Fixed	10 μm
	σ_{eff}	Fixed	0.1 μm

Note: For definitions of the parameters and references for the “a priori values” used see reference 27 (Sanz-Requena et al., 2018)

Supplementary Table 3

Radiative transfer model best-fitting parameters

Parameter	***Reference Latitude 69°N***	***Storm Latitude***
τ_{str}	0.02±0.01	0.04±0.01
P_{bot}/z	320±50mbar/57±5km	270±50 mbar/65 ±5km
τ_{trop}	10±2	33±2
τ_{cloud}	7±2	8±2
N_{max}	49±10 par/cm3	216±10 par/cm3
$H_{aerosol}/H_g$	0.5±0.1	0.3±0.1
r_{eff}	0.10±0.1 µm	0.18±0.1 µm

Supplementary Table 4.1

Parameter	***Range of values***
Mass volume injection (m^3/s)	2×10^8 - 4×10^{10}
WS1 planetographic latitude (degrees)	66.5° - 67.5°
WS2 planetographic latitude (degrees)	68.5° - 69.0°
Gaussian Perturbation radius (degrees)	0.5 - 2
Gaussian Perturbation size (degrees)	0.5 - 2
Layer depth (m)	500 - 5000
Resolution (degrees/pixel)	0.1
Domain	65° x 72.5° Latitude - 360° Longitude

Shallow Water model simulations: parameter space ranges

Supplementary Table 4.2

EPIC model simulations: parameter space ranges

Parameter	***Range of values***	***Range of values***
Case study	WS1 + WS2	Cyclone + WS1
Gaussian perturbation heat seed (W/kg)	0.1 - 5	1 – 3 (for WS1)
Gaussian perturbation size (degrees)	0.1 - 0.35	1.5x0.5 (Cyclone) 0.1 - 0.2 (WS1)
WS1 planetographic latitude (degrees)	66.5 - 67.5	67 - 68.5
WS2 planetographic latitude (degrees)	68.5 - 69.3	---------
Resolution (degrees/pixel)	0.06 - 0.23	0.06 - 0.23

Domain	65° x 72.5° Latitude - 240° Longitude
Layers	N = 5 (Altitude range = 200 mb – 500 mb)

Note: Simulations were performed for two cases. Two simultaneous storms (WS1+WS2) and a storm inside a cyclone (Cyclone +WS1).

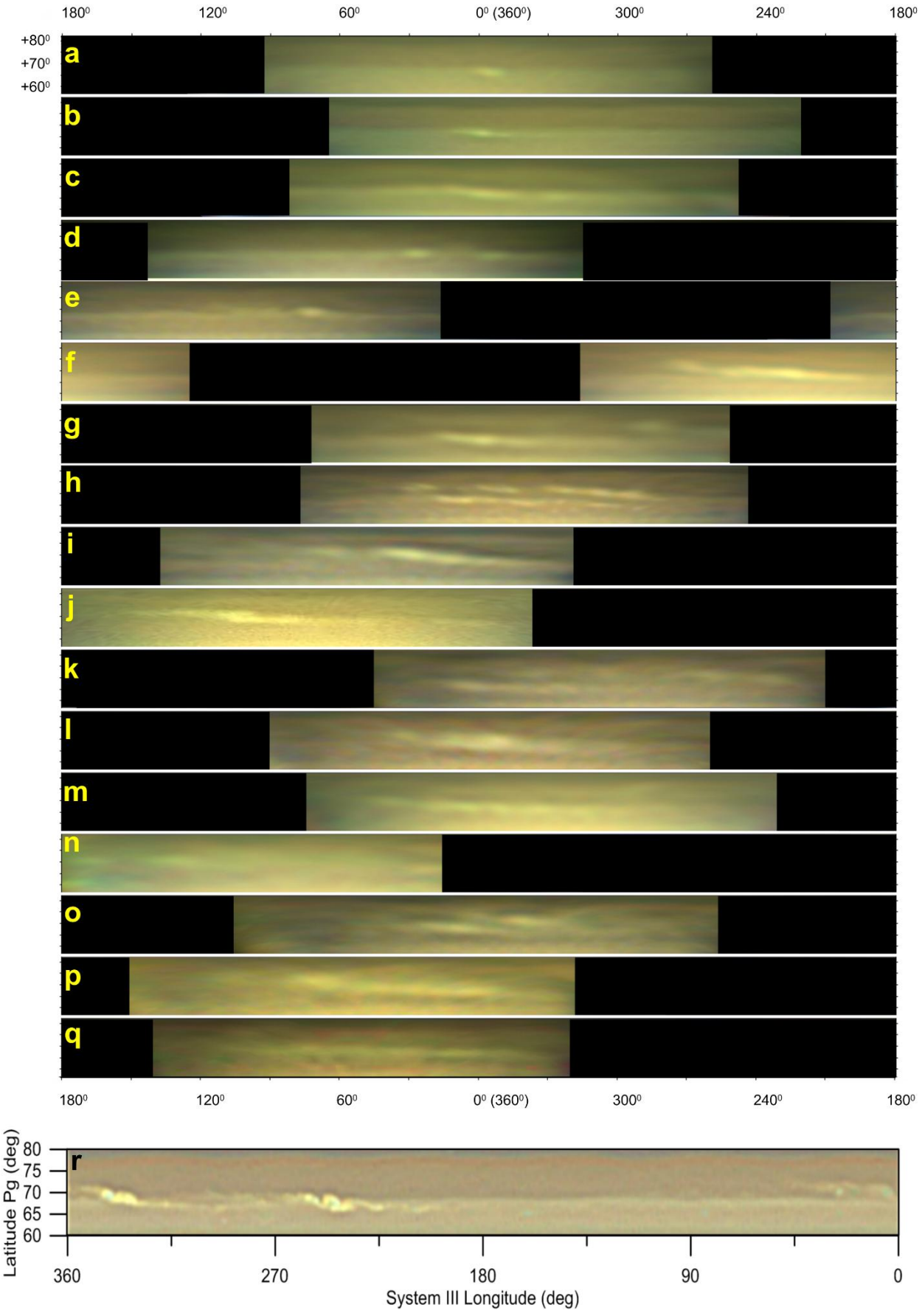
180⁰
120⁰
60⁰
0⁰ (360⁰)
300⁰
240⁰
180⁰
+80⁰
+70⁰
+60⁰
a
b
c
d
e
f
g
h
i
j
k
l
m
n
o
p
q
r
Latitude Pg (deg)
80
75
70
65
60
360
270
180
90
0
System III Longitude (deg)

Supplementary Figure 1. (a-q) Evolution of polar storm from ground-based map projected images. Maps are equirectangular projections of a strip around +68°N planetographic latitude (Y-axis). *L'* Longitudes (X-axis) are in a modified system based on the drift of the first detected spot (WS1) to have it always around 0°, given by *L'* = *L*3 – (299.7° - 11.618°/*d* *(T – 2018 June 01.5)). The acquisition time (year 2018 and time in U.T.) and observer for each strip (see Table S1) are: (a) March 29, 08:16:06 (M. Sparrenberger); (b) April 01, 08:54:62 (D. Peach); (c) May 18, 16:07:00 (T. Barry); (d) May 26 14:52:48 (A. Casely); (e) June 02, 16:38:00 (D. Pfitzner Milika); (f) June 22, 12:38:54 (A. Casely); (g) June 23, 13:14:00 (T. Barry); (h) June 30, 13:13:00 (D. Pfitzner Milika); (i) July 11, 03:14:30 (B. MacDonald); (j) July 19, 22:12:40 (S. Voltmer); (k) August 04, 01:59:18 (B. MacDonald); (l) August 05, 02:06:48 (B. MacDonald); (m) August 19, 10:35:00 (T. Barry); (n) August 31, 20:00:00 (J. Camarena); (o) September 16, 00:59:48 (B. MacDonald); (p) September 23 23:48:48 (B. MacDonald); (q) November 03, 17:08:00 (C. Foster). The original images have been reprocessed to prepare the maps in order to have a similar rendering. The first map (2018-03-29) shows the first image of the polar storm (WS1 persistent spot close to longitude 0°). It spread rapidly, developing tails towards NW and SE (2018-04-01), following the wind profile at those latitudes. (r) Cylindrical map from HST-WFPC using System III longitudes from images obtained on June 6.

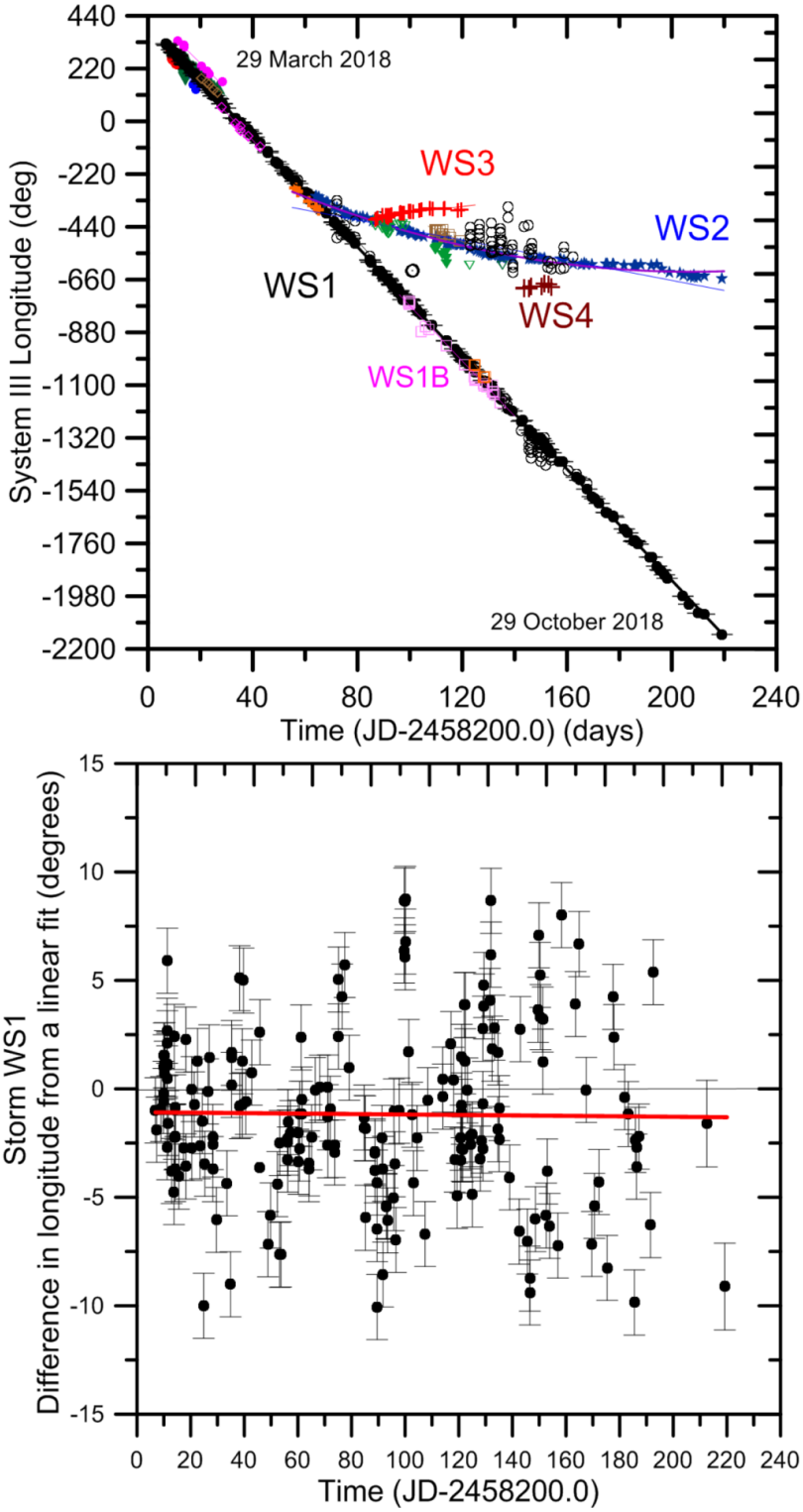

Supplementary Figure 2. Top: Drift in System III Longitude of the main storms tracked along 2018. Bottom: Difference in longitude relative to a linear drift for storm WS1. The error bars in the individual longitude points are calculated from the errors introduced in the planet limb navigation and feature pointing. The estimated longitude error for each individual feature is ±2°.

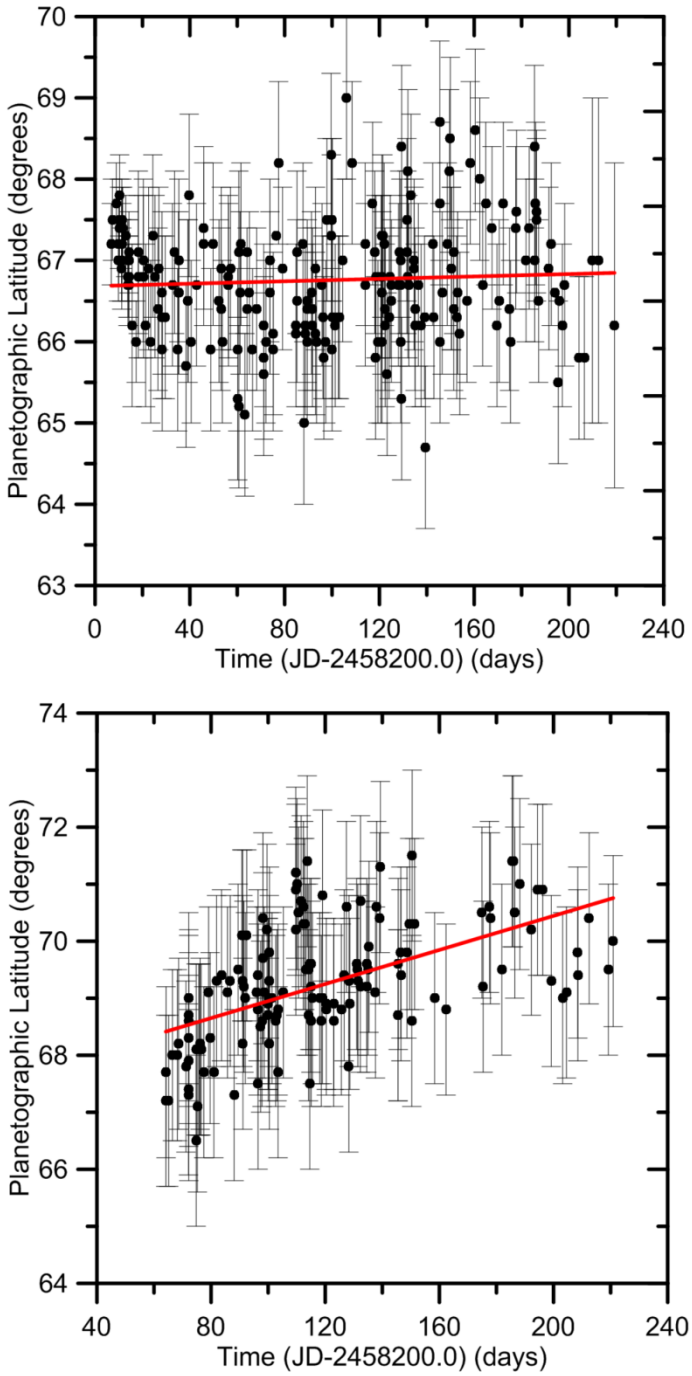

Supplementary Figure 3. Top: Latitude vs time of storm WS1. Bottom: Latitude vs time of storm WS2. The red line are linear fits to the data points. The error bars in the individual latitude points are calculated from the errors introduced in the planet limb navigation and feature pointing. The estimated latitude error for each individual feature is ±2°.

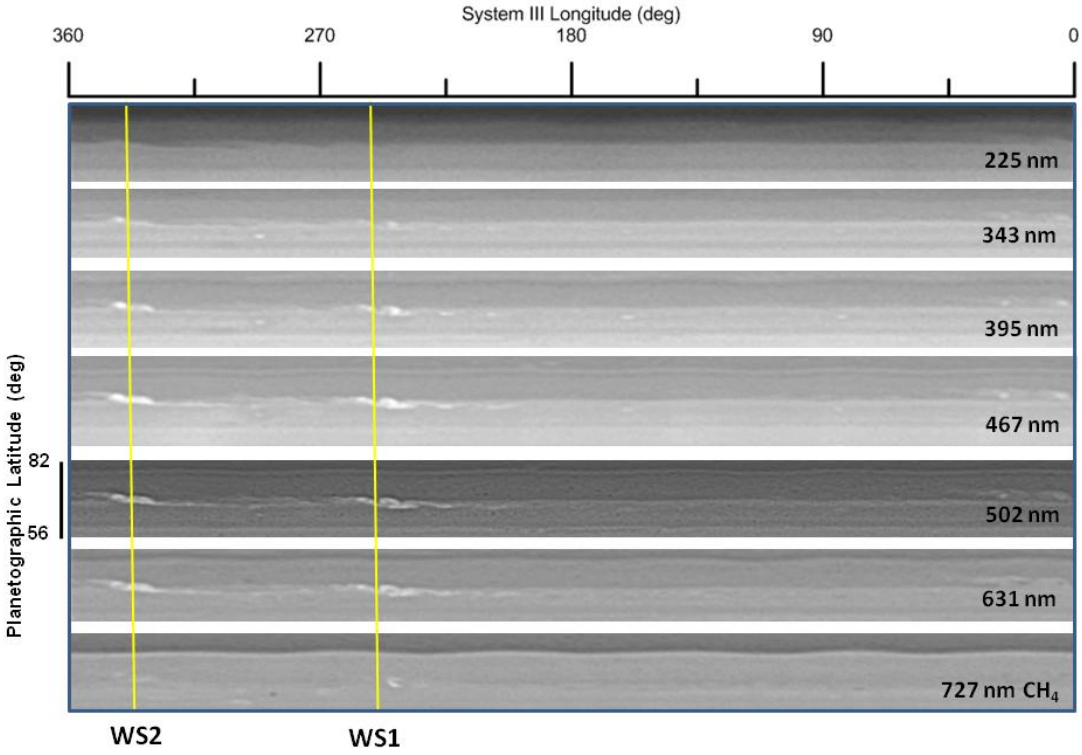

Supplementary Figure 4. Cylindrical map projection strips showing the storms WS1 and WS2 at different wavelengths as observed on 6 June 2018 using the WFPC camera on Hubble Space Telescope (from OPAL program). Each strip is built from a composition of several images obtained over one planetary rotation.

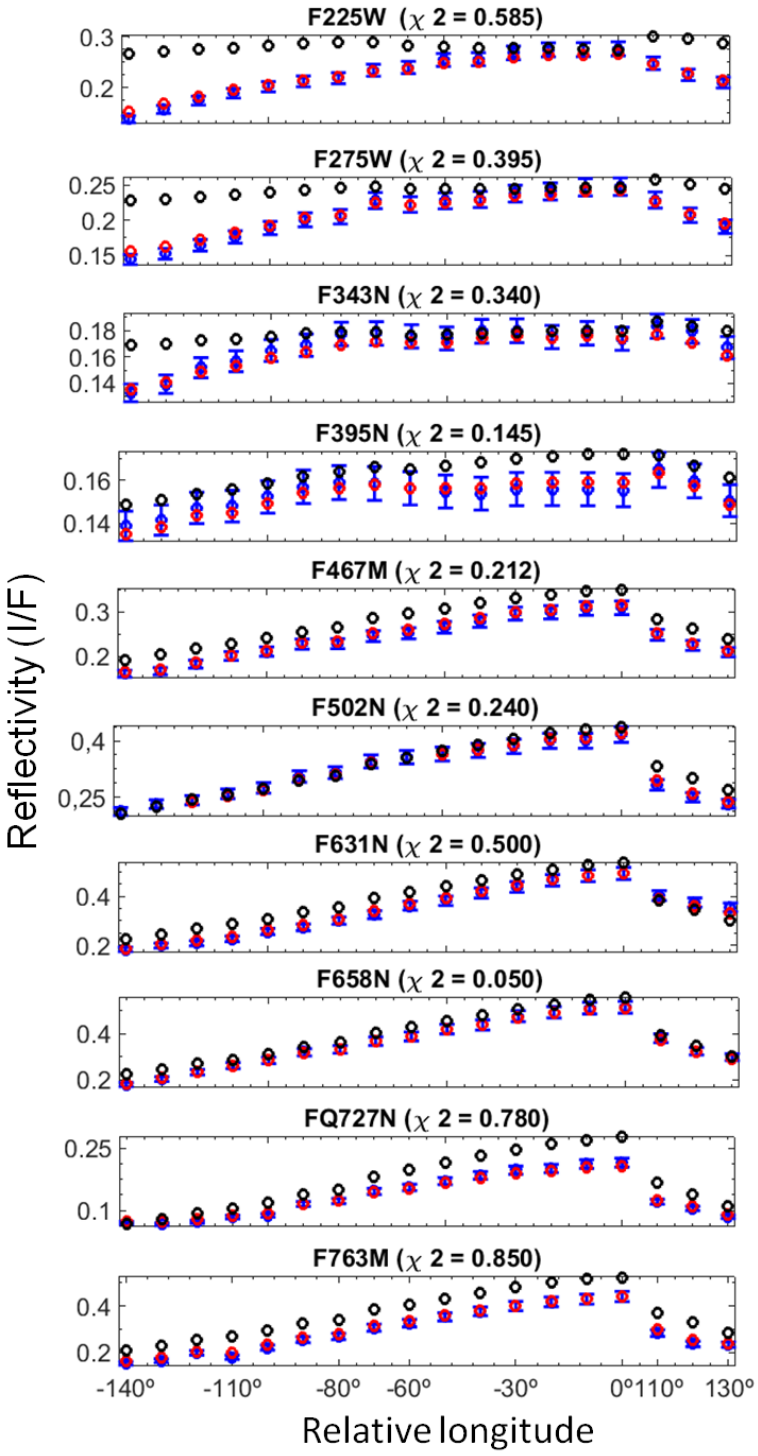

Supplementary Figure 5. Center to limb dependence of the reflectivity of the storm WS1 with wavelength (blue dots with error bars) compared to the radiative transfer model (red dots). The circles indicate the reflectivity from the "a priori" particle density assumed for the model retrieval. The χ^2 value indicates the goodness of the fit.

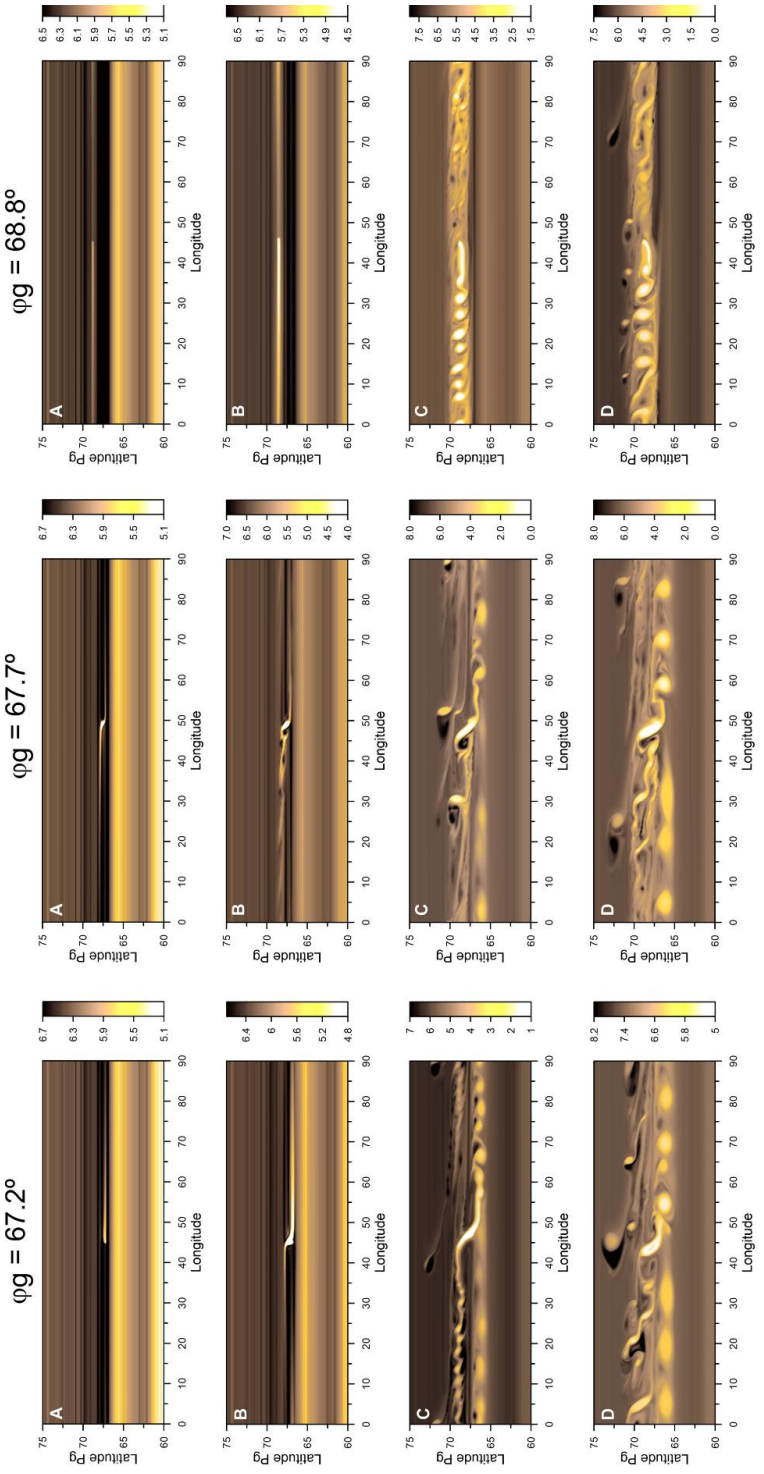

Supplementary Figure 6. Potential vorticity maps (10^{-7} m-^{1}s^{-1}) resulting from numerical simulations of the Shallow Water model of a storm outbreak for different mass flow injection at different latitudes as indicated. The mass flow injection values are Q (m^{3}s^{-1}) = A (4x10^8), B (2x10^9), C (2x10^{10}), D (4x10^{10}). The best agreement corresponds to Q = 2-4x10^9 m^{3}s^{-1} and latitude φ_g = 67.7°. The disturbance moves with a velocity of +59.8 ms^{-1} in System III reference frame.

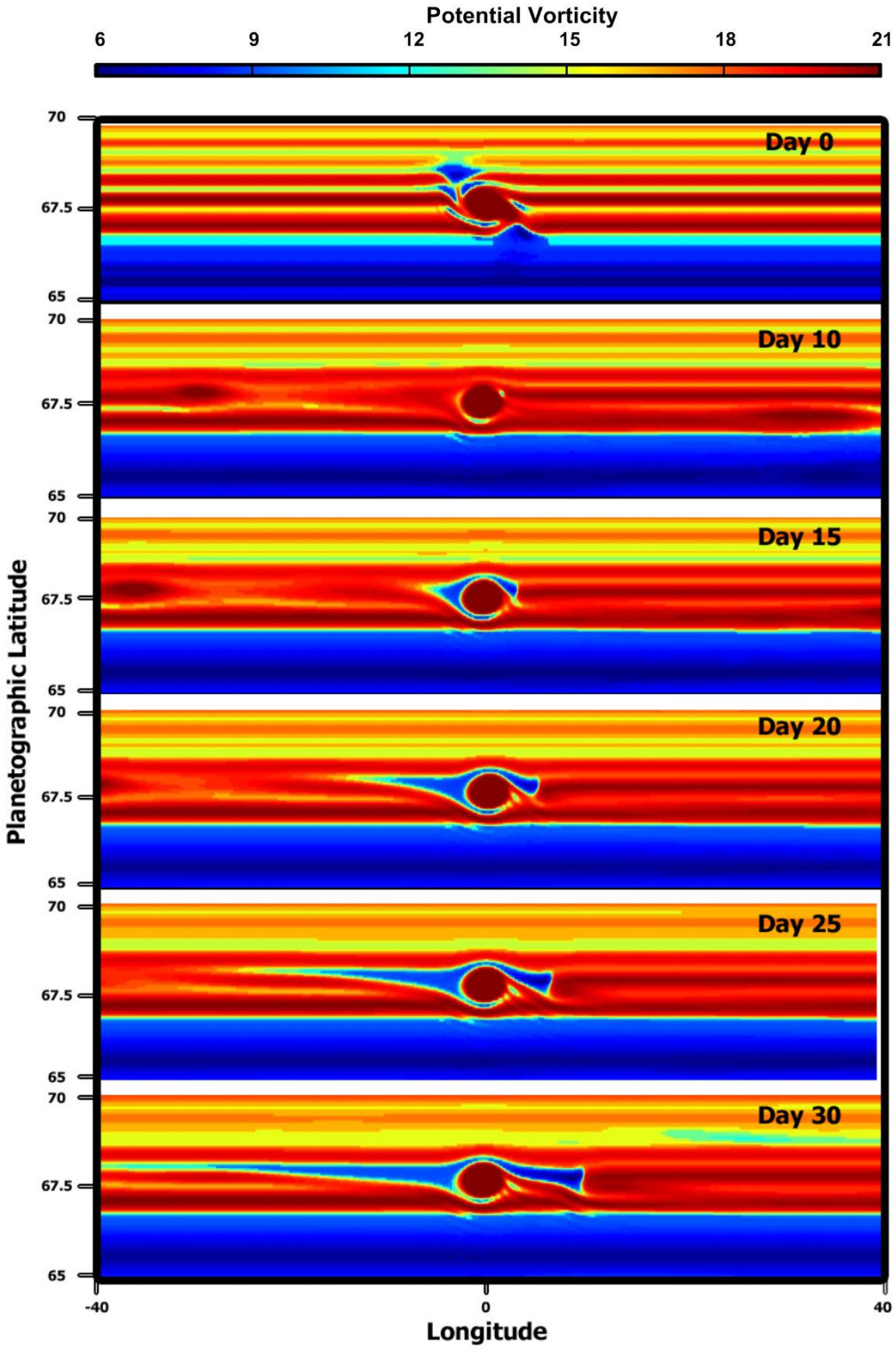

Supplementary Figure 7. Ertel Potential Vorticity (EPV, 10^{-6} $Kkg^{-1}m^2s^{-1}$) maps resulting from numerical simulations of the EPIC model of a storm outbreak in the interior of a cyclone. The cyclone has 1.5° x 0.5° (longitude x latitude) and a storm with a Gaussian shape with a size of 0.15° x 0.1° and heating intensity of 1 W kg^{-1} is continuously introduced since day 10. The heating is active along the simulation period, introduced in each time step and moving with the cyclone speed.

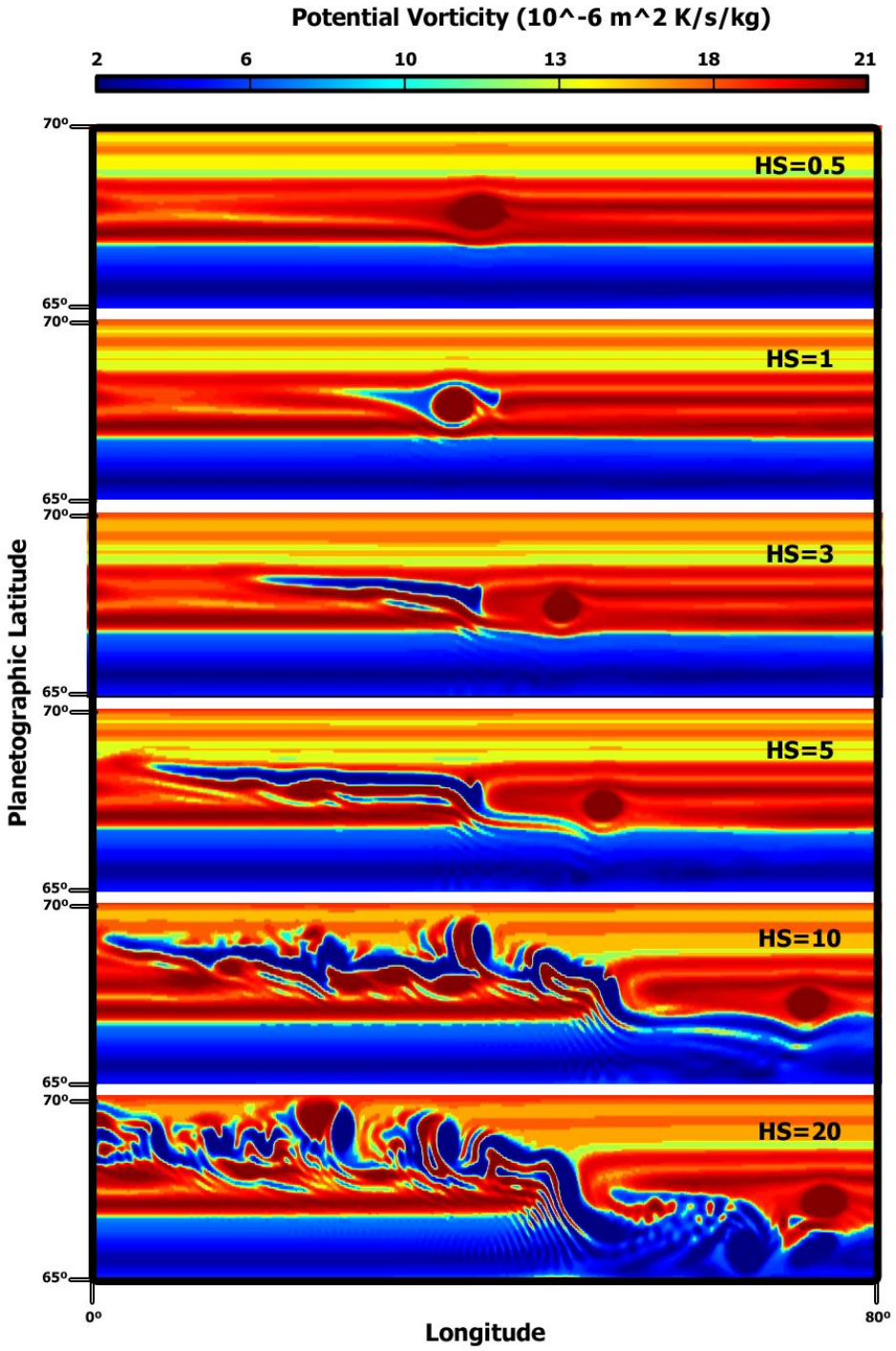

Supplementary Figure 8. Ertel Potential Vorticity (EPV) maps resulting from numerical simulations of the EPIC model of a storm outbreak in the interior of a cyclone as in Figure S7 but changing the Heating Source intensity HS = 0.5 to 20 W kg^{-1} as indicated. The maps represent EPV at day 20 of the simulation.

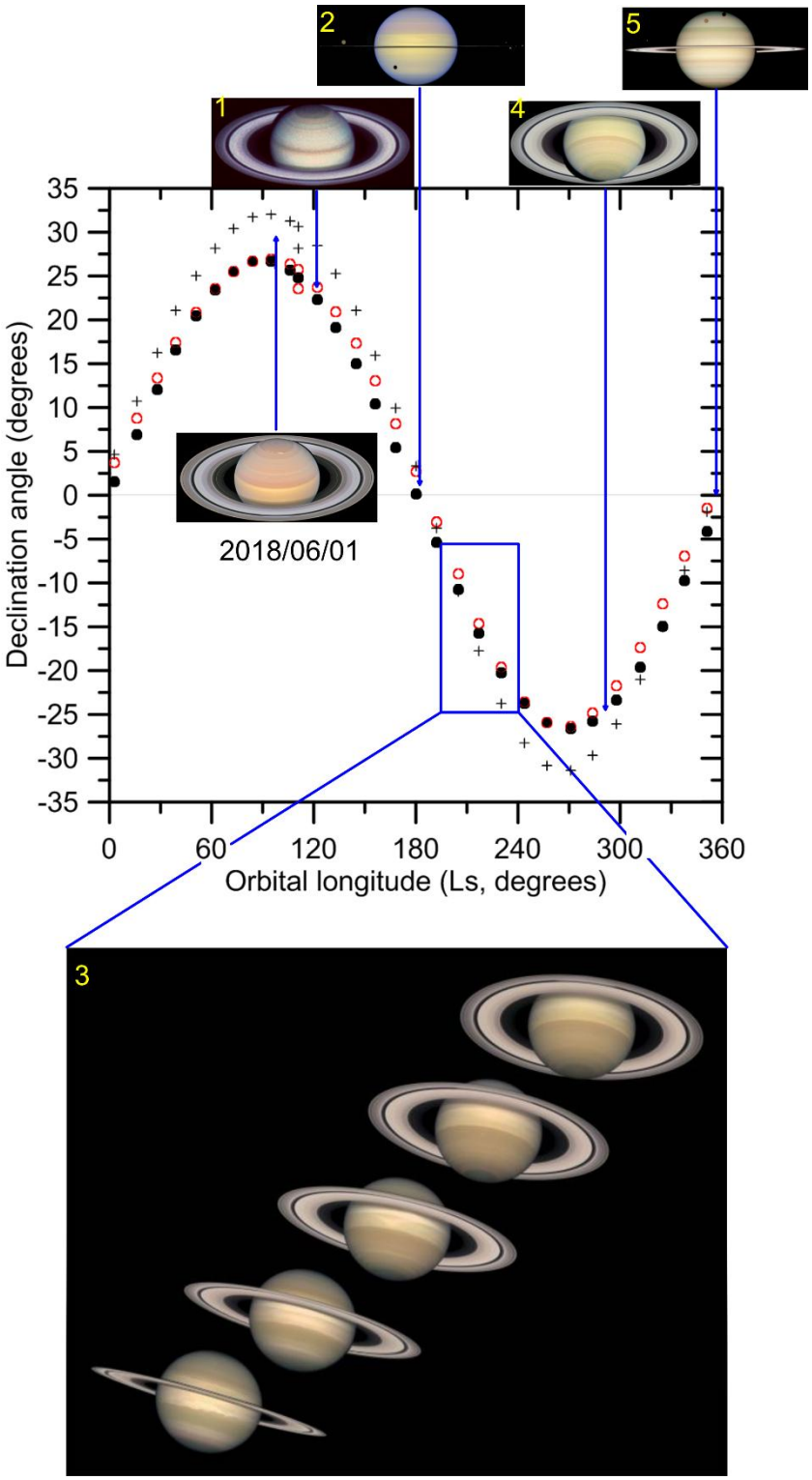

Supplementary Figure 9. Hemispheric visibility of Saturn along its year represented in terms of the declination angle (black dots) and the orbital longitude (L_s). Black dots: Declination of the Sun; red circles: declination of the Earth; crosses: planetographic latitude of the center of the disk. Representative images from Hubble Space Telescope: (1) 26 August 1990; (2) 6 August 1995; (3) From bottom to top: October 1996, October 1997, October 1998, October 1999, October 2000; (4) 22 March 2004; (5) 24 February 2009. The observation corresponding to the storms is indicated by the date (1 June 2018).